

Radius of Robust Feasibility for Ground Coverage in Aerial Sensor Networks

Vanshika Datta^a, C. Nahak^a

^a*Department of Mathematics, Indian Institute of Technology Kharagpur, Kharagpur, West Bengal, India-721302*

Abstract

Sensors are vital for environmental monitoring, yet their effectiveness diminishes under spatial uncertainty. We propose a robust optimization framework for maximizing the coverage of aerial directional sensors under spatial uncertainty. Each sensor projects a truncated sector on the ground, parameterized by its altitude, field of view, and orientation. To address sensor displacement uncertainty, we introduce the radius of robust feasibility (RRF) as a measure of tolerance against positional perturbations. We formulate an exact expression for the RRF of aerial sensor networks and embed it into the coverage maximization model as a robustness constraint. Our approach guarantees that the optimized configuration remains feasible under bounded uncertainty. A distributed greedy algorithm based on Voronoi partitioning is used for orientation adjustment, ensuring scalable and adaptive deployment toward high-impact regions. Experimental results validate the effectiveness of our model in preserving robust coverage across complex terrain and varying uncertainty conditions.

Keywords: Radius of robust feasibility; Voronoi diagram; Directional sensor network; Data uncertainty

MSC: 49K99; 65K10; 90C29; 90C46; 90C34

1. Introduction

Sensors possess the inherent ability to perceive, record, and react to their surrounding environment. This fundamental capability underpins their widespread application in diverse domains such as airport surface surveillance, border monitoring, disaster response, smart agriculture, infrastructure inspection, and urban traffic management [1, 2]. As sensors evolved from passive data collectors to active decision-making agents, wireless sensor networks (WSNs) emerged as a critical infrastructure for real-time monitoring in resource-constrained environments [3, 4].

Within the broader class of WSNs, directional sensor networks (DSNs) have attracted significant attention due to their use of limited-angle sensors, such as cameras, infrared, ultrasonic, and LiDAR, offering focused coverage with higher precision [5, 6]. These directional sensors necessitate not only optimal placement but also strategic orientation to ensure maximum effective coverage, making the deployment problem inherently more complex than in traditional omnidirectional WSNs [7]. This complexity is further amplified in aerial sensor networks (ASNs), wherein sensors are mounted on unmanned aerial vehicles (UAVs) or drones and deployed in three-dimensional space. Their sensing footprints, projected onto the ground, are typically fan-shaped and depend heavily on altitude and yaw angle [2, 3].

However, a major challenge across these settings is uncertainty, stemming from sensor placement errors, localization drift, environmental disturbances, or communication inaccuracies. In cluttered or GPS-denied environments such as dense forests or disaster zones, such uncertainties can significantly degrade sensing performance, resulting in coverage gaps, misaligned orientation, energy inefficiency, and compromised communication [8, 9]. Although grid-based and geometric deployment methods have attempted to optimize coverage [6, 10, 11], they often assume precise sensor positioning, rendering them fragile under even small perturbations.

While many efforts have focused on energy-efficient design and network longevity [12, 13], the deployment strategies themselves must also be resilient to uncertainty. Traditional probabilistic methods such as stochastic

*Corresponding author

Email address: cnahak@maths.iitkgp.ac.in (C. Nahak)

programming require accurate distributional assumptions, which are often unavailable in field deployments. This motivates the need for robust optimization (RO), a paradigm that accounts for uncertainty in a deterministic yet conservative manner. [14, 15]

Robust optimization explicitly incorporates uncertainty sets within optimization models, producing solutions that remain feasible across all realizations of uncertainty within those sets. Originating from Soyster’s foundational work [16] and advanced through tractable frameworks by Ben-Tal, Nemirovski, and El Ghaoui [14, 17, 18], RO has matured into a powerful methodology applicable across continuous, discrete, and mixed-integer domains [19, 20, 21, 22]. Its value is particularly evident in high-stakes or data-sparse environments, where conservative feasibility is prioritized over nominal optimality [23]. RO enables declarative statements like, “I do not know exactly where the sensor is, but I require the coverage constraint to be satisfied regardless of its exact position within an uncertainty region.”

Yet a persistent challenge within RO is determining the threshold of uncertainty that a given solution can tolerate. Here, the radius of robust feasibility (RRF) plays a crucial role. RRF encapsulates the greatest size of an uncertainty set such that a desirable property, such as constraint feasibility, is preserved regardless of the parameter realization. Originally proposed by Goberna et al. [24] for linear semi-infinite programs (LSIPs), this concept has significantly evolved to encompass convex, nonconvex, and mixed-integer frameworks, see [23] and the references therein.

The RRF offers not just a theoretical foundation but also a practical tool for designing systems that retain functionality under worst-case scenarios, which is often more critical than optimizing for ideal conditions. The radius essentially delineates the largest possible uncertainty set, typically modeled as a norm ball or more general convex set, within which the robust counterpart remains feasible, thereby ensuring system reliability, see [25]. Furthermore, the distinction between different types of radii, such as the radius of highly robust weakly efficient solutions for multi-objective convex programs [24], and the radius of robust feasibility for constraint-focused optimization [26], underscores the versatility of this concept. The latter, which forms the basis of our work, serves as a computational threshold ensuring that robust feasible solutions exist across all admissible perturbations. Applications of RRF now span from gas network control and facility location design to wireless and distributed sensor networks, proving its value in domains where preserving system operability under uncertainty is paramount [27].

In the context of distributed sensor networks, where sensor deployment often faces imprecision due to terrain irregularities, environmental noise, or mobility, the integration of RRF provides a rigorous mechanism to tolerate spatial uncertainty. Instead of assuming perfect placement, RRF enables one to model a tolerance region, allowing small displacements without violating feasibility [3]. This leads to robust strategies that enhance system resilience while preserving coverage quality.

As Ridolfi et al. [28] have recently demonstrated, transitioning from uncertain coefficients to uncertain locations marks a significant breakthrough, enabling new insights in location-based optimization. The RRF offers a powerful geometric and optimization-based lens through which to examine robustness. Given the energy constraints of sensor networks, an uncertainty-aware approach is essential for optimizing data collection while ensuring long-term network sustainability. A robust design, rather than one solely focused on optimality under fixed conditions, enhances the adaptability of DSNs across varying uncertainty scenarios, reinforcing the importance of incorporating RRF into DSN modeling.

In this paper, we extend the RRF paradigm to aerial directional sensor networks, a class of DSNs where each sensor is mounted at a fixed height and projects a directional sensing truncated cone onto the ground. This formulation is particularly applicable to UAV-based surveillance, environmental monitoring, and disaster response. Building upon the Voronoi-based greedy orientation framework introduced in prior work [7], we propose an uncertainty-aware optimization model that strategically orients sensors to maximize coverage, while ensuring robust feasibility under bounded sensor displacement.

Our contributions can be summarized as follows:

- We formulate a nominal coverage maximization model for aerial DSNs and extend it into a robust optimization framework that explicitly accounts for location uncertainty using RRF.
- We generalize the results of 2D directional sensor networks [29] to aerial sensor networks by projecting the 3D sensing geometry onto the ground plane and deriving the corresponding coverage constraints.

- If the nominal solution exhibits insufficient robustness, we introduce a constraint to enforce a minimum RRF, thereby obtaining a robustified configuration.
- Our algorithm employs a Voronoi-partitioned, distributed greedy orientation strategy that adapts to dynamic conditions without requiring global information.
- Through comprehensive simulations, we analyze how key parameters: sensor count, field of view, sensing radius, and uncertainty bounds, influence coverage and robustness.

This work bridges a notable gap in the literature. Although robust optimization has previously addressed uncertainty in sensor networks [3], most models either assume isotropic sensors or rely on probabilistic models. The application of RRF in directional aerial sensor networks with uncertain locations remains unexplored. Our model avoids probabilistic assumptions, offers provable robustness guarantees, and enhances adaptability in uncertain, real-world scenarios.

The remainder of this paper is structured as follows. Section 2 reviews related works on sensor coverage, robustness under uncertainty, and radius of robust feasibility. Section 3 presents the modeling framework and problem setup, including preliminaries, sensor geometry, sensing model, uncertainty characterization, and formulation of nominal and robustified optimization models. Section 4 introduces the orientation adjustment strategy for coverage enhancement, classifies Voronoi–projection intersection cases, analytically computes the covered area for each case, and proposes a distributed orientation optimization algorithm. Section 5 provides experimental evaluation and validates the model through simulations across various scenarios and performance setups. It demonstrates the practical effectiveness and resilience of our model. Section 6 concludes the paper with major findings, limitations, and directions for future research.

2. Related Works

Robust optimization has long been a cornerstone in handling uncertainty across domains, including wireless and directional sensor networks. However, most traditional work relies on probabilistic models or static assumptions, which limit applicability in dynamic, real-world scenarios. Below, we position our work relative to existing literature across three key themes: uncertainty modeling via RRF, coverage maximization in sensor networks, and robust optimization frameworks in sensing.

2.1. Modeling the notion of RRF to handle data uncertainty

The RRF, introduced by Goberna et al. [24, 30], serves as a fundamental tool in robust optimization, providing guarantees on feasibility under data perturbations. While early formulations primarily focused on LSIP and ball uncertainty sets [31, 32], later works generalized RRF to broader uncertainty structures, including spectrahedral and convex compact sets [33, 34, 35, 36]. Notably, Ridolfi and Serio [28] explored RRF in uncertain farthest Voronoi cells, moving toward spatial interpretations of robustness. However, none of these works applied RRF to directional sensing, let alone aerial 3D environments.

Our model builds upon Ridolfi’s geometric insight, extending it to directional sensor networks (DSNs) with 3D spatial uncertainties. Unlike [37], which derived RRF for traditional linear programs, we derive an exact RRF formulation, tackling 3D space, embedding it into a continuous orientation strategy, and incorporating an optimization layer to maximize uncertainty-resilient coverage. Furthermore, we introduce an uncertainty updating mechanism that adapts to deployed sensor locations, an aspect not considered in prior work. For a comprehensive survey and recent developments on the radius of robust feasibility, one may refer to [26, 38]. While some recent efforts, such as [39, 40, 41], address computational tractability or mixed-integer robustness, our focus is distinct in applying RRF to aerial DSN orientation under spatial uncertainty.

2.2. Maximizing coverage in sensor networks

Coverage optimization in sensor networks, particularly directional sensor networks, has been extensively studied [4, 5, 7]. Most work focuses on optimizing orientation or placement [1, 2], but does not integrate robustness into the formulation. Liu et al. [1] addressed deployment of directional cameras for airport surface

surveillance using truncated sector models and adaptive orientation strategies. However, their model assumes deterministic conditions and boundary constraints without addressing location uncertainty.

Our work differs in three major aspects. First, we extend Sung et al.'s sector-based model to 3D aerial projections [7], enabling coverage across complex terrains. Second, we incorporate uncertainty directly into the optimization problem using RRF-based formulations. Third, we develop a Voronoi-partitioned, distributed greedy orientation strategy that operates in dynamic, unconstrained environments, such as aerial sensor networks, [1]. Unlike [3], which addresses distance uncertainty in energy-limited WSNs using probabilistic models within a robust optimization framework, our approach focuses on spatial location uncertainty and employs deterministic, RRF-based robust formulations tailored for aerial directional sensor orientation under 3D uncertainty. Furthermore, our work marks the first integration of exact RRF computation and constraint-based enforcement in 3D aerial sensor networks.

2.3. Handling data uncertainty in optimization frameworks

Robust optimization in sensing has predominantly focused on energy-efficiency [27], consistency [25], or constraint-level perturbations [42]. Few works integrate RRF within directional sensing, particularly in 3D. Our earlier work [29] introduced RRF to DSNs in 2D, using linearized models. While it demonstrated feasibility, it lacked scalability and applicability to aerial environments.

This paper significantly advances our prior work by extending the RRF-based model to 3D aerial sensor networks. We develop a continuous optimization framework that embeds robust feasibility directly. Inspired by boundary-critical models and adaptive learning methods, we incorporate real-time adaptability into our model. Together, these advances allow our method to address coverage, orientation, and robustness simultaneously in volatile, real-world environments. Moreover, one may refer to [5] for related approaches in cooperative sensing.

Our contribution is distinct in integrating the radius of robust feasibility with directional sensing, emphasizing sensor location uncertainty rather than uncertain coefficients. The incorporation of RRF into a distributed orientation strategy renders our framework both theoretically rigorous and practically applicable in uncertain 3D environments, such as aerial surveillance and terrain monitoring. By fusing it with the foundational principles of directional sensor networks enabling iterative refinement and real-time optimization, our model presents a novel, scalable, and robust solution for efficient sensor placement under spatial uncertainty and resource limitations.

3. Modeling framework and problem setup

This section introduces the theoretical modeling and optimization framework for robust coverage in aerial directional sensor networks under uncertainty. We present formal notations, define the sensing geometry, construct Voronoi-based decomposition, and integrate the RRF into a robust optimization scheme.

3.1. Preliminaries and notation

Let $\mathbb{R}^n, \mathbb{B}_n, \|\cdot\|$ denote respectively, the n -dimensional Euclidean space, the open unit ball and Euclidean norm. The transpose of a vector a is denoted by a^T , and the Euclidean distance between $x, y \in \mathbb{R}^n$ is $d(x, y) = \|x - y\|$. For a set $S \subset \mathbb{R}^n$, we denote its closure, convex hull, and conical hull by $cl(S)$, $conv(S)$, and $cone(S)$, respectively. The relative interior and dimension of a convex set S are denoted by $rint(S)$ and $dim(S)$. Functions $r : S \rightarrow \mathbb{R}_+$ form the space \mathbb{R}_+^S , and finitely supported functions $\lambda : S \rightarrow \mathbb{R}_+$ form $\mathbb{R}_+^{(S)}$.

Lemma 3.1. (Schur complement [37], Lemma 2.1) *Let $W = \begin{bmatrix} A & B^T \\ B & C \end{bmatrix}$ be symmetric with $A \succ 0$. Then $W \succeq 0$ if and only if $C - BA^{-1}B^T \succeq 0$.* ■

Definition 3.1. (Reference cone [36]) *Given a linear system $\sigma := \{a_s^T x \leq b_s, s \in S\}$, its reference cone K is defined as:*

$$K := clcone \left\{ \begin{bmatrix} a_s \\ b_s \end{bmatrix}, s \in S; \begin{bmatrix} 0_n \\ 1 \end{bmatrix} \right\}.$$

A parametric linear system in the face of data uncertainty in its constraints, denoted by σ^α , can be captured as follows:

$$\sigma^\alpha := \{a_s^T x \leq b_s, s \in S\}; (a_i, b_i) \in \mathcal{U}_i^\alpha \subset \mathbb{R}^{n+1}; i = 1 : p,$$

where (a_i, b_i) for $i = 1 : p$ are uncertain vectors and \mathcal{U}_i^α ; $i = 1 : p$ are the uncertain regions, which are typically assumed to be compact and convex.

The robust counterpart (deterministic form) of the corresponding system σ^α with $U_i^\alpha = (\bar{a}_s, \bar{b}_s) + \alpha B_{n+1}$, $s \in S$, $i = 1 : p$ and the corresponding feasible set F_R^α for some $\alpha \in \mathbb{R}$ is:

$$\sigma_R^\alpha := \{a_s^T x \leq b_s, \forall (a_i, b_i) \in U_i^\alpha, s \in S\}.$$

The radius of robust feasibility ρ , of an uncertain system σ^α , determines the maximum level of perturbation that a system can tolerate while remaining feasible. It is formally defined as follows:

Definition 3.2. (Radius of robust feasibility) Consider a parametric linear system in face of data uncertainty σ^α . Let F_R^α denote the feasible set of the robust counterpart of σ^α . Then, the RRF for the system is given by:

$$\rho = \sup\{\alpha \in \mathbb{R}_+ : (F_R^\alpha) \text{ is nonempty}\}.$$

This quantifies the maximum perturbation level under which the system remains robustly feasible. A fundamental concept in computing RRF is the Minkowski function, defined as follows:

Definition 3.3. (Minkowski function) Let $\omega \subset \mathbb{R}^n$ be a convex set containing 0_n in its interior. Then the Minkowski or gauge function of ω denoted by ϕ_ω , where $\phi_\omega : \mathbb{R}^n \rightarrow \mathbb{R}_+ := [0, +\infty[$ is given by:

$$\phi_\omega(x) := \inf\{t > 0 : x \in t\omega\}, x \in \mathbb{R}^n.$$

The following lemma provides some properties of the Minkowski function.

Lemma 3.2 (See [37], Lemma 2.2). Let $\omega \subset \mathbb{R}^n$ be a convex set such that its interior contains 0_n , then the following properties hold:

- (1) ϕ_ω is sublinear and continuous.
- (2) $\{x \in \mathbb{R}^n : \phi_\omega(x) \leq 1\} = cl(\omega)$, where $cl(\omega)$ stands for the closure of ω .
- (3) If in addition, ω is bounded and symmetric, then $\phi_\omega := \|\cdot\|$ is a norm on \mathbb{R}^n generated by ω . ■

The next lemma defines a dual characterization of solutions of a semi-infinite linear inequality system, which is useful for our analysis in the sequel. It is found in [43].

Lemma 3.3. Let I be an arbitrary index set. Then,

$$\{x \in \mathbb{R}^n : a_i^T x \leq b_i : i \in I\} \neq \emptyset \iff (0_n, 1) \notin clcone \{(-a_i, -b_i) : i \in I\}. \quad \blacksquare$$

The next lemma is an extension of [31], which uses the epigraphs of conjugate functions of convex functions.

Lemma 3.4. Let $\alpha \in \mathbb{R}_+$ and $(a_i, b_i) \in \mathbb{R}^{n+1}; i = 1 : p$. Also, let \mathcal{U}_i^n be the uncertain sets in \mathbb{R}^{n+1} as discussed above. If

$$(0_n, 1) \in clcone \left\{ \bigcup_{i=1}^p [(-\bar{a}_i, -\bar{b}_i) - \alpha \mathcal{U}_i^n] \right\}$$

holds, then for all $\delta > 0$, we have

$$(0_n, 1) \in cone \left\{ \bigcup_{i=1}^p [(-\bar{a}_i, -\bar{b}_i) - (\alpha + \delta) \mathcal{U}_i^n] \right\}.$$

Exact formula of RRF for an arbitrary set $S \subset \mathbb{R}^{n+1}$ has been obtained in literature in terms of the so-called hypographical set $H(\bar{a}, \bar{b})$ of the nominal system σ :

$$H(\bar{a}, \bar{b}) := conv \{(-\bar{a}_i, -\bar{b}_i) : i = 1 : p\} + \mathbb{R}_+(0_n, -1),$$

where $\bar{a} = (\bar{a}_1, \bar{a}_2, \dots, \bar{a}_p) \in (\mathbb{R}^n)^p$ and $\bar{b} = (\bar{b}_1, \bar{b}_2, \dots, \bar{b}_p) \in \mathbb{R}^p$.

Theorem 3.5. *If the nominal system is feasible, the RRF of σ^α is:*

$$\rho = \inf_{(a,b) \in H(\bar{a},\bar{b})} \phi_Z(a,b),$$

where $Z \subset \mathbb{R}^n$ is a convex and compact set containing 0_n in its interior, see [37].

Definition 3.4. (Voronoi cell) *Given a set of generator points $S = \{s_1, s_2, \dots, s_n\}$ in \mathbb{R}^2 , the Voronoi cell $V_S(s_i)$ associated with sensor $s_i \in S$ is defined as:*

$$V_S(s_i) = \{p \in \mathbb{R}^2 : d(p, s_i) \leq d(p, s_j) \text{ for all } j \neq i\},$$

where $j = 1 : n$ and $d(a, b)$ is the Euclidean distance between a and b .

A Voronoi diagram is a spatial decomposition of a region based on proximity to a given set of points, called generators (sensor nodes in our case). It consists of the union of all Voronoi cells (see Figure 1).

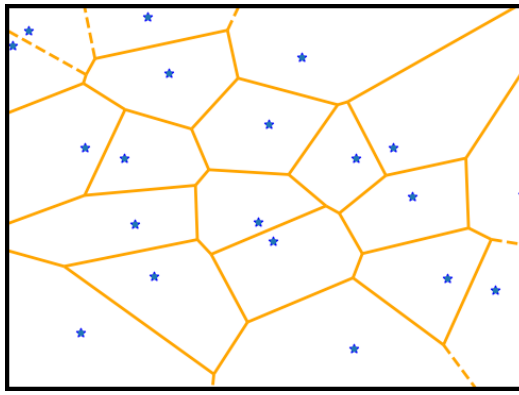


Figure 1: Voronoi diagram for a set of generators

3.2. Sensor geometry and sensing model

We analyze a directional sensing model where sensors are positioned in 3D space at $(x_s, y_s, z_s) \in \mathbb{R}^3$, typically elevated to expand the field of view and mitigate occlusion effects, resulting in a top-down orientation as illustrated in Figure 2a. The sensor's horizontal and vertical angles of view are denoted by θ_H and θ_V , respectively. Its tilt is defined as the angle α between the camera's optical axis and the xy-plane, which controls vertical inclination, while β_s specifies the horizontal orientation with respect to the x-axis, where $\beta_s = 0$ indicates alignment along x.

Given the sensor's position $(x_s, y_s, z_s) \in \mathbb{R}^3$ and tilt angle α_s (relative to the xy-plane), the sensing region forms an irregular rectangular pyramid, as illustrated in Figure 2. To analyze ground coverage, we project this 3D volume orthogonally onto the xy-plane, resulting in a truncated sector or fan-shaped footprint, shown in Figure 2b. Each aerial directional sensor s , mounted at a known altitude, is defined in 2D by its location (x_s, y_s) , orientation β_s (relative to the x-axis), and angular view θ_H . The inner and outer sensing radii are denoted r_s and R_s , respectively. The ground projection $A_s(\beta_s)$ corresponding to this footprint is defined as:

$$A_s(\beta_s) = \left\{ (x, y) \in \mathbb{R}^2 \mid r_s \leq \|(x, y) - p_s\| \leq R_s, \arctan 2(y - y_s, x - x_s) \in \left[\beta_s - \frac{\theta_H}{2}, \beta_s + \frac{\theta_H}{2} \right] \right\}, \quad (3.1)$$

where, $\arctan 2(y - y_s, x - x_s)$ denotes the angle between the vector from sensor s to point (x, y) and the positive x-axis.

Let $T \subset \mathbb{R}^3$ denote the set of aerial sensors with $|T| \geq 2$, and fix a sensor $t \in T$ located at (x_s, y_s, z_s) . Since coverage is evaluated on the ground plane, we project the 3D sensing volume onto the xy-plane; we henceforth consider only the sensor's planar coordinates (x_s, y_s) , denoted by $s \in S$ where S is the projection of T onto the x-y plane. Let $p = (x, y) \in \mathbb{R}^2$ represent a point on the ground. The point p is said to be covered by the sensor s if it lies within both the radial and angular constraints of its field of view. The effective sensing region is thus an annular sector defined by the parameters $(r_s, R_s, \theta_H, \beta_s)$.

Specifically, sensor s covers point p if the following two conditions are met:

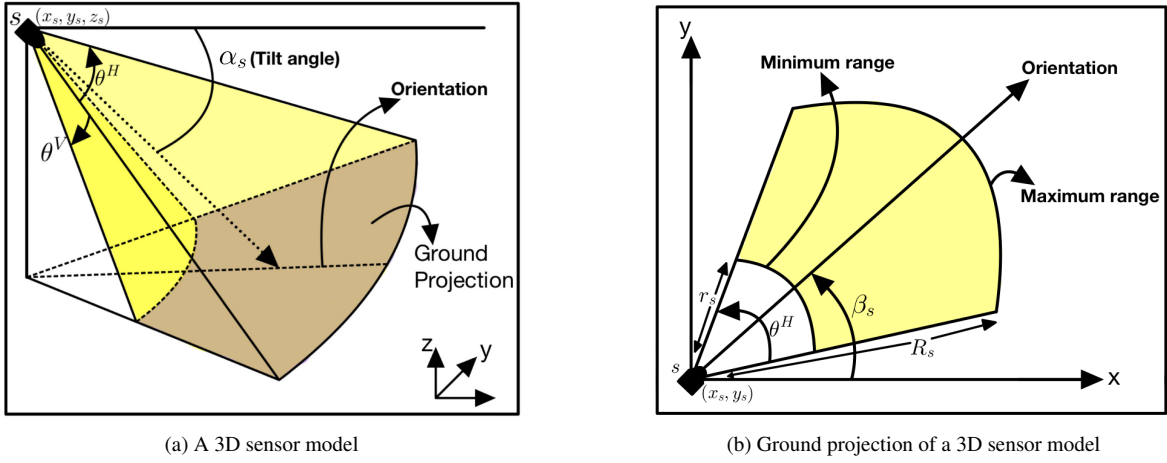


Figure 2: Sensing model in 3D and its ground projection

(1) The Euclidean distance from p to the sensor lies within the sensor's detection range:

$$r_s \leq \sqrt{(x - x_s)^2 + (y - y_s)^2} \leq R_s.$$

(2) The angle between the sensor's forward orientation β_s and the direction vector \vec{sp} is within the sensor's angular field of view:

$$|\text{atan2}(y - y_s, x - x_s) - \beta_s| \leq \frac{\theta_H}{2}.$$

3.3. Optimization models under uncertainty

Now consider throughout the paper that we have m sensors in a sensor set $S = \{s_1, s_2, \dots, s_m\} \subset \mathbb{R}^2$ with atleast two specific sensors $s, t \in S$, which are characterized by its location after the ground projection, i.e. $s = (x_s, y_s), t = (x_t, y_t) \in S$. Each sensor is responsible for covering its own Voronoi cell, leveraging the fact that a sensor has maximum inductive capacity within its cell. Due to the convexity of Voronoi cells, Theorem 3.2 of [29] ensures that the farthest point from a sensor within its cell is towards one of its vertices. Hence, to enhance ground coverage using directional sensors under positional uncertainty, we present a three-stage modeling and optimization framework. This includes the nominal model (with and without uncertainty), its robust formulation, and the robustified optimization approach integrating the RRF concept.

3.3.1. Nominal and uncertainty model

$$VC(s) = \{p \in \mathbb{R}^2 : \|p - s\| \leq \|p - t\|, \forall t \in S\}.$$

Note that we have to enhance the overall coverage, for that we need to maximize the total area covered by all the sensors together, subject to the constraints such as the overlap of sensing area, out of interest boundary coverage, etc. For this, we consider the Voronoi diagram of all the sensors in the set S and maximize the area covered by each sensor inside its corresponding Voronoi cell.

Now, consider throughout the paper that $I_j = \{1, 2, \dots, n_j\}$ represents the index set corresponding to sensor s_j for $j = 1 : m$, where n_j denotes the number of vertices in the Voronoi cell of s_j . The vertices of the Voronoi region associated with sensor s_j for $i = 1 : n_j$ are denoted as $v_{j,i}$. The area covered by s_j within its Voronoi region when oriented towards vertex $v_{j,i}$ is represented as $A_{j,i}$. Furthermore, let V_j and A_j denote the optimal orientation vertex selected and the corresponding covered area for sensor s_j within its Voronoi region, respectively, for $j = 1 : m$.

Hence, we get the following nominal optimization model:

$$\text{Model 1 (Nominal): } \max \sum_{j=1}^m A_j(s_j), \quad (3.2)$$

subject to the following constraints for each nominal $s_j \in S$:

$$A_j(s_j) \subseteq VC(s_j) := \{p \in \mathbb{R}^2 : \|p - s_j\| \leq \|p - s_i\|, \forall s_i \in S\} \quad (\text{Voronoi cell constraint}), \quad (3.3)$$

$$A_j(s_j) \subseteq A_{s_j}(\beta_{s_j}) \quad (\text{Sensing region constraint}), \quad (3.4)$$

$$A_j(s_j) \subseteq \text{ROI} \quad (\text{Boundary constraint}), \quad (3.5)$$

where $A_{s_j}(\beta_{s_j})$ is as defined in equation (3.1) and ROI is the region of interest. Note that this optimization model is the nominal one which ensures the maximum coverage obtained by the set of sensors S leveraging each sensor's Voronoi cell while accounting for the out-of-boundary coverage avoidance. Note that the above nominal model does not account for uncertainty in sensor positioning, hence it does not ensure robust feasible coverage. Hence, in the next subsection, we discuss its robust counterpart (RC).

3.3.2. Robust counterpart under location uncertainty

Consider the coverage model in the face of location uncertainty of sensors. Then, each sensor $s_j \in S = \{s_1, s_2, \dots, s_m\}$ having the nominal location \bar{s}_j will belong to the uncertainty set \mathcal{U}_j^α ; $j = 1 : m$, defined by:

$$\mathcal{U}_j^\alpha := \bar{s}_j + \alpha \mathbb{B}_2; i = 1 : n, \quad (3.6)$$

where \mathbb{B}_2 denotes the closed unit ball in \mathbb{R}^2 , which is convex and compact with $0_2 \in \text{int}(\mathbb{B}_2)$.

Hence, we incorporate location uncertainty into the model and the RC of the nominal model in Section 3.3.1 becomes:

$$\max \sum_{j=1}^m A_j(s_j), \quad (3.7)$$

subject to the following constraints for all $s_j \in \mathcal{U}_j^\alpha$:

$$A_j(s_j) \subseteq VC(s_j) := \{p \in \mathbb{R}^2 : \|p - s_j\| \leq \|p - s_i\|, \forall s_i \in S\} \quad (\text{Voronoi cell constraint}), \quad (3.8)$$

$$A_j(s_j) \subseteq A_{s_j}(\beta_{s_j}) \quad (\text{Sensing region constraint}), \quad (3.9)$$

$$A_j(s_j) \subseteq \text{ROI} \quad (\text{Boundary constraint}), \quad (3.10)$$

where $A_{s_j}(\beta_{s_j})$ is as defined in equation (3.1) and ROI is the region of interest.

To ensure robust coverage, we consider the worst-case area of each sensor's coverage region A_j under uncertainty. To do this, we need to get the worst-case location of each sensor $s_j \in S$ with respect to its uncertainty set \mathcal{U}_j^α . Note that we consider the Voronoi cell with respect to the nominal location of sensors. It is easy to see that the worst-case (minimum) coverage occurs when the sensor lies on the boundary of its uncertainty region; hence, we have the following lemma:

Lemma 3.1 (Coverage Under Uncertainty). *For a convex uncertainty ball \mathcal{U}_j , the minimum area covered by a sensor $s_j \in S$ is achieved at the boundary of \mathcal{U}_j .*

Assuming the nominal system, say σ_o , is feasible, we now define the worst-case sensor position ' s_{jw} ' for sensor $s_j \in S$ along the direction of sensing \vec{u} , which gives a meaningful and tractable representation for robust coverage analysis:

$$s_{jw} = \bar{s}_j + \alpha \frac{\vec{u}}{|\vec{u}|}.$$

Using this worst-case location along with equation (3.6) in the above robust counterpart, we get the following deterministic robust model of our problem:

$$\text{Model 2 (RC): } \max \sum_{j=1}^m A_j(s_{jw}), \quad (3.11)$$

subject to the following constraints for each worst case location s_{jw} of sensor $s_j \in \mathcal{U}_j^\alpha$:

$$A_j(s_{jw}) \subseteq VC(s_j) := \{p \in \mathbb{R}^2 : \|p - s_j\| \leq \|p - s_i\|, \forall s_i \in S\} \quad (\text{Voronoi cell constraint}), \quad (3.12)$$

$$A_j(s_{jw}) \subseteq A_{s_j}(\beta_{s_{jw}}) \quad (\text{Sensing region constraint}), \quad (3.13)$$

$$A_j(s_{jw}) \subseteq \text{ROI} \quad (\text{Boundary constraint}). \quad (3.14)$$

This becomes a deterministic model that ensures coverage remains feasible for all perturbations in \mathcal{U}_j^α as it ensures the same for the worst case s_{jw} . While it incorporates uncertainty, it does not quantify robustness, so solutions may still fail when location errors exceed certain limits. To address this, in the next subsection, we compute the RRF of the obtained solution; if it falls below a set threshold, an RRF-constrained optimization is invoked to redesign orientations, guaranteeing resilience against deviations up to the specified magnitude.

3.3.3. Formulation of robustified optimization model

To quantify the degree of robustness and explicitly enforce a measurable resilience margin, we introduce the concept of RRF into this optimization framework. Let σ_j^α denote the system of constraints in the Model 2 for the sensor $s_j \in S; j = 1 : m$ with corresponding robust feasible set \mathcal{F}_j^α . Then, in the sequel of Definition 3.2, see [29], we have the RRF definition as:

Definition 3.5 (RRF for directional sensor). *Let S be a set of sensors in a DSN with $s_j \in S$. Then, RRF of s_j is defined as the largest non-negative radius α such that the coverage constraints remain satisfied for all perturbations in the enlarged uncertainty set \mathcal{U}_j^α , given by equation (3.6). i.e.*

$$\rho_{s_j} = \sup \{\alpha \in \mathbb{R} \geq 0 : \mathcal{F}_j^\alpha \neq \emptyset \forall j = 1 : m\}.$$

Thus, the RRF serves as a direct measure of the robustness margin of a given solution. Also, we have the following theorem to calculate the exact RRF for the sensor $s_j \in S$.

Theorem 3.1 (Exact RRF formula [29], Theorem 3.1). *If the nominal system is feasible, then the RRF of sensor $s_j \in S$ is given by:*

$$\rho_{s_j} = \inf_{x \in \mathcal{F}_j^\alpha} \min_i \frac{\bar{b}_i - \bar{a}_i^T x}{\xi_{\mathcal{U}_j^\alpha}(x, -1)},$$

where $\xi_{\mathcal{U}_j^\alpha}(x, -1)$ is the support function of the uncertainty set \mathcal{U}_j^α , given by equation (3.6) capturing worst-case directional perturbation.

Now, we consider the third model, which integrates the RRF directly into the model by imposing the RRF constraints, where r_{\min} is a user-defined robustness threshold. As a result, the optimization model not only accounts for worst-case uncertainty (as in the previous model) but also guarantees that the solution remains feasible for any location deviations up to r_{\min} beyond the nominal uncertainty bounds. The resulting formulation is:

$$\text{Model 3 (Robustified): } \max \sum_{j=1}^m A_j(s_{jw}), \quad (3.15)$$

subject to the following constraints for each worst case location s_{jw} of sensor $s_j \in \mathcal{U}_j^\alpha$:

$$A_j(s_{jw}) \subseteq VC(s_j) := \{p \in \mathbb{R}^2 : \|p - s_j\| \leq \|p - s_i\|, \forall s_i \in S\} \quad (\text{Voronoi cell constraint}), \quad (3.16)$$

$$A_j(s_{jw}) \subseteq A_{s_j}(\beta_{s_{jw}}) \quad (\text{Sensing region constraint}), \quad (3.17)$$

$$\rho_{s_j} \geq r_{\min} \quad (\text{RRF constraint}), \quad (3.18)$$

$$A_j(s_{jw}) \subseteq \text{ROI} \quad (\text{Boundary constraint}). \quad (3.19)$$

Thus, this model ensures that the orientation is optimized under modeled location uncertainty and is also provably resilient to location perturbations of magnitude at least ρ_{\min} . Note that this model introduces a tradeoff between coverage and robustness: the larger the guaranteed RRF, the more conservative the footprint, potentially reducing coverage but improving feasibility under perturbations. Furthermore, it results in a robustified design ensuring minimum robustness.

3.4. Problem overview and solution flow

We address robust coverage optimization for aerial directional sensors, each projecting a truncated sector on the ground with adjustable orientation. The problem considers a particular region, random deployment, Voronoi partitioning, and wedge-shaped sensing regions with uncertain inner/outer radii. Using the RRF concept, we adjust sensor locations to their worst-case values, reformulate the original optimization into a deterministic robust model, and solve it. The workflow (Figure 3) integrates performance optimization, RRF computation, and re-optimization if the RRF falls below a threshold, ensuring guaranteed robustness without assuming probabilistic location errors.

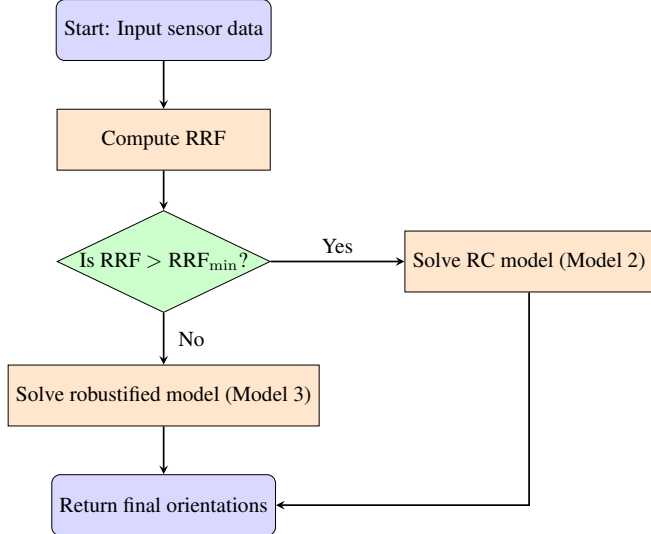


Figure 3: Flowchart for RRF-based robust sensor orientation framework

4. Orientation adjustment strategy for coverage enhancement

Our aim is to model directional sensing under perturbations, quantify robustness via the RRF, and formulate an optimization problem ensuring resilient coverage. Following Sung et al. [7], we use Voronoi diagrams and direction-adjustable sensors to design an adaptive, distributed placement strategy for improved coverage in directional sensor networks. As described in Section 3.2, a point is covered if it meets two conditions, which in the robust case are evaluated using the sensor's robust location. For the j^{th} sensor s_j , $j = 1 : m$, located at nominal coordinates (x_s, y_s) with RRF ρ_{s_j} and oriented toward vertex $V = (a, b)$, the direction vector is $\vec{\mu} = (a - x_s, b - y_s)$. Normalizing and scaling by the RRF gives the robust location $s_{jw} = (x'_s, y'_s)$:

$$\begin{aligned}
 (x'_s, y'_s) &= (x_s, y_s) + \rho_{s_j} \frac{\vec{\mu}}{|\vec{\mu}|} \\
 &= (x_s, y_s) + \rho_{s_j} \left(\frac{a - x_s}{\sqrt{(a - x_s)^2 + (b - y_s)^2}}, \frac{b - y_s}{\sqrt{(a - x_s)^2 + (b - y_s)^2}} \right). \tag{4.1}
 \end{aligned}$$

A point $p(a_0, b_0)$ is covered by s_j if $r_s \leq d(s_{jw}, p) \leq R_s$ and $\omega \leq \frac{\theta_H}{2}$, where r_s , R_s , and θ_H are the minimum range, maximum range, and angular coverage of s_j , and ω is the angle between \vec{sp} and $\hat{\mu}$. If β_s is the angle between $\hat{\mu}$ and the positive x -axis, $-\pi \leq \beta_s \leq \pi$, the second condition yields:

$$\begin{aligned}
 \vec{sp} \cdot \hat{\mu} &= ||\vec{sp}|| ||\hat{\mu}|| \cos \omega \\
 \implies (a_0 - x'_s) \cos \beta_s + (b_0 - y'_s) \sin \beta_s &= \sqrt{(a_0 - x'_s)^2 + (b_0 - y'_s)^2} \cos \omega \\
 \implies (a_0 - x'_s) \cos \beta_s + (b_0 - y'_s) \sin \beta_s &\geq \sqrt{(a_0 - x'_s)^2 + (b_0 - y'_s)^2} \cos \frac{\theta_H}{2}. \tag{4.2}
 \end{aligned}$$

Thus, under the robust case, $p(a_0, b_0)$ is covered if it satisfies $r_s \leq d(s_{jw}, p) \leq R_s$ and (4.2).

4.1. Classification of Voronoi-projection intersection cases

Consider the Voronoi diagram of a set of sensors S . Also, let a particular sensor $s \in S$. The coverage region of the sensor is bounded between its two sensing range arcs and the span angle or the sector sidelines. To ensure each sensor achieves maximum coverage, the coverage area associated with its robust location is calculated for every candidate vertex, and the orientation providing the largest coverage is chosen as the optimal direction. The area calculation is performed within the bounds of the sensor's own Voronoi cell. Let the inner and outer arcs of the sensor's coverage sector be denoted by s_{in} and s_{out} , respectively. Based on the interactions between the Voronoi edges, sensing arcs, and the sector sidelines, seven distinct geometric configurations arise:

- 1 No Voronoi-edge intersection with either arc or the sidelines.
- 2 Voronoi-edge intersection with s_{out} and a sideline.
- 3 Voronoi-edge intersection with s_{in} and a sideline.
- 4 Voronoi-edge intersection with only the sidelines from inside the sense range.
- 5 Voronoi-edge intersection with only the sidelines from outside the sense range.
- 6 Voronoi-edge intersection with both arcs s_{in} and s_{out} as well as the sidelines.
- 7 No intersection with any boundary element.

4.2. Analytical computation of covered area for each case

To maximize the overall coverage of sensor network, we need to compute the area sensed by each sensor inside its Voronoi cell and maximize it. For the first case of no Voronoi-edge intersection with either arc or the sidelines, we can simply use the sector area formula and calculate the required sensing region area as the difference of outer and inner sector region:

$$A_j = \frac{\theta_H}{2} r_s'^2,$$

where θ_H is the sensor's field of view in radians and r_s' is its effective coverage range, which is given by the difference of outer and inner range of corresponding sensor s_j , $j = 1 : m$, i.e. $R_s - r_s$.

For the other cases, we consider N number of Voronoi vertices inside the Voronoi cell of a specific sensor $s \in S$. We find the area by constructing line segments between the sensor's robust location s_{jw} and the intersection points of the sector boundaries with the Voronoi edges. The coverage area is computed by dividing the region into $N + 1$ triangles formed by connecting the sensor location to each vertex. For this, the sensor's robust position is connected via line segments to all intersection points of the sector arcs and sidelines with Voronoi edges. Doing so, we get either a triangle, a sector or truncated sector sensing region.

The area of each triangle is obtained using Heron's formula:

$$\text{Area of a triangle} = \sqrt{d(d - e_1)(d - e_2)(d - e_3)}, \quad (4.3)$$

where $d = \frac{e_1 + e_2 + e_3}{2}$ is the semiperimeter and e_i ; $i = 1 : 3$ are the triangle's edges.

The Voronoi vertices and edges are known from the Voronoi diagram, while the intersection points with the sector sidelines are derived by first formulating the sector sideline equations. Clearly, we get the sector sideline equation when the equality in equation (4.2) holds. Therefore, for a sensor s_j nominally located at (x_s, y_s) with a robust position $s_{jw} = (x'_s, y'_s)$, orientation angle β_s and the minimum and maximum effective sensing ranges r_s and R_s , respectively, the sector sideline equations are given by:

$$\begin{cases} (a_o - x'_s) \cos \beta_s + (b_o - y'_s) \sin \beta_s = \sqrt{(a_o - x'_s)^2 + (b_o - y'_s)^2} \cos \frac{\theta_H}{2}, \\ r_s \leq d(t_j, p) \leq R_s. \end{cases} \quad (4.4)$$

Given the sensor's robust position $s_{jw} = (x'_s, y'_s)$, the minimum and maximum effective sensing ranges r_s and R_s , respectively, angle of view θ_H and orientation angle β_s , the area is calculated using the sector arc equations:

$$\begin{cases} d(s_{jw}, p) = r_s, \\ a_0 \in [r_s \cos\left(\beta_s + \frac{\theta_H}{2}\right) + x'_s, r_s \cos\left(\beta_s - \frac{\theta_H}{2}\right) + x'_s], \\ b_0 \in [r_s \sin\left(\beta_s - \frac{\theta_H}{2}\right) + y'_s, r_s \sin\left(\beta_s + \frac{\theta_H}{2}\right) + y'_s] \end{cases} \quad (4.5)$$

and

$$\begin{cases} d(s_{jw}, p) = R_s, \\ a_0 \in [r_s \cos\left(\beta_s + \frac{\theta_H}{2}\right) + x'_s, r_s \cos\left(\beta_s - \frac{\theta_H}{2}\right) + x'_s], \\ b_0 \in [r_s \sin\left(\beta_s - \frac{\theta_H}{2}\right) + y'_s, r_s \sin\left(\beta_s + \frac{\theta_H}{2}\right) + y'_s], \end{cases} \quad (4.6)$$

where $p = (a_0, b_0)$ denotes a point located on the arc boundary of the sensor's coverage sector. After computing the desired coverage area for all cases, the sensor selects a unit direction vector pointing toward the vertex that provides the maximum coverage. This vector is chosen as the optimal orientation direction. If two or more sensors have same vertex as optimal orientation, the one with lesser coverage reorient itself to the next best vertex to minimize the overlaps.

4.3. Proposed orientation optimization algorithm

We propose an algorithm that integrates sensor orientation optimization with robustness evaluation based on the radius of robust feasibility, see algorithm 1. Unlike traditional approaches, our method begins by computing the RRF for each sensor in the given configuration. If the minimum RRF among each sensor meets or exceeds a predefined robustness threshold (ρ_{\min}), the algorithm proceeds to solve the robust counterpart model (Model 2, see equation (3.11)), which accounts for worst-case perturbations in sensor positions while optimizing orientations under constraints such as orientation bounds and overlap limits.

If the minimum RRF is below the threshold, the algorithm instead solves a robustified model (Model 3, see equation (3.15)) that explicitly enforces $\text{RRF} \geq \rho_{\min}$ for each sensor, ensuring that the resulting configuration is resilient against worst-case location deviations up to the specified robustness requirement. This conditional strategy avoids unnecessary conservatism and computational overhead by applying the stricter robustness constraint only when required. For practical demonstration, we consider identical sensors with the same angle of view and field of coverage, and the proposed method efficiently balances optimal coverage performance with guaranteed resilience to sensor location uncertainty.

5. Experimental analysis

This section presents a comprehensive experimental evaluation of the proposed RRF-based robustified sensor orientation framework. We first compare sensor coverage under nominal and perturbed deployments to demonstrate the effect of robustness on overall performance. This is followed by a Voronoi-cell-wise analysis, which highlights how coverage is distributed across individual sensors. Finally, we investigate the influence of varying sensing parameters, providing insights into the sensitivity and trade-offs introduced by robustification.

5.1. Scenario setup

We consider a randomized deployment of m aerial directional sensors $S = \{s_1, \dots, s_m\}$ within a bounded square region \mathbf{R} of size 1000×1000 units. Each sensor s_i is assigned a sensing field characterized by an angular view θ_H , and its effective ground coverage is determined relative to its associated Voronoi cell when the sensor is projected as a point onto the plane. This modeling approach ensures that the ground region is partitioned equitably, with each sensor responsible for covering the area that is closer to it than to any other sensor. Although we present results under a common value of θ_H , the formulation is flexible and can be readily extended to accommodate heterogeneous angular ranges across different sensors, thereby enhancing the applicability of the analysis to more practical scenarios. The overarching optimization objective is to maximize the effective

Algorithm 1 Integrated Sensor Orientation Optimization with RRF-based Robustness Evaluation

Require: Number of sensors m , initial positions $S = \{s_1, \dots, s_m\}$, sensing range bounds r_s and R_s , maximum overlap ϵ , minimum change in overall area δ , minimum RRF threshold ρ_{\min} , sensing angle θ_H

Ensure: Final optimal robust sensor orientations and corresponding maximum coverage

- 1: **Step 1: Initialization**
- 2: Set initial sensor positions S and orientations
- 3: Compute initial Voronoi diagram for S
- 4: Set $\rho^* = \min_i \rho_i^*$
- 5: **Step 2: Robustness Assessment**
- 6: **for** each sensor s_j **do**
- 7: Compute RRF ρ_{s_j} using Theorem 3.1
- 8: **end for**
- 9: **Step 3: Voronoi-based Local Refinement**
- 10: **for** each sensor $s_j \in S$ **do**
- 11: Identify Voronoi vertices for s_j within allowable region
- 12: For each vertex, compute coverage area at worst-case location
- 13: Select orientation maximizing coverage for s_j
- 14: **end for**
- 15: **Step 4: Robust Coverage Optimization (Model 2) or Robustified Re-Optimization (Model 3)**
- 16: **for** each sensor $s_j \in S$ **do**
- 17: **if** $\rho_{s_j} > \rho_{\min}$ **then**
- 18: Formulate and solve Model 3.11 (RC without RRF constraint) subject to (3.12), (3.13) and (3.14).
- 19: Record candidate robust orientations and coverage
- 20: **else**
- 21: Add RRF constraint to optimization model 3.11 to get its robustified version.
- 22: Formulate and solve Model 3.15 subject to (3.16), (3.17), (3.18) and (3.19).
- 23: Record candidate robust orientations and coverage
- 24: **end if**
- 25: **end for**
- 26: **Step 5: Cooperative Recalibration**
- 27: **repeat**
- 28: **for** each pair (s_i, s_j) sharing a Voronoi vertex **do**
- 29: **if** overlap is more than threshold $(\rho_{s_i} + \rho_{s_j} + R_{s_i} + R_{s_j} - d_{ij} > \epsilon)$ **then**
- 30: Compare coverage areas A_i and A_j
- 31: Sensor with smaller coverage reorients to next-best vertex
- 32: **end if**
- 33: **end for**
- 34: **until** No further beneficial adjustments possible (Overall change in area is lesser than δ threshold)
- 35: **Output:** Final sensor orientations and coverage satisfying $\text{RRF} \geq \rho_{\min}$ if required.

coverage contributed by the sensor of each Voronoi cell and, consequently, the total network coverage, while simultaneously accounting for deployment uncertainties and mitigating redundant overlaps.

To discourage inefficient redundancy, a threshold parameter λ is introduced: whenever the effective area covered by a sensor directed toward one of its Voronoi vertices falls below λ , that orientation is deemed non-contributory and hence discarded. In cases where no feasible vertex orientation exists, the sensor is either assigned a randomized angular direction or switched to a sleep mode, thereby conserving energy and extending the overall network lifetime. The iterative optimization proceeds by sequentially maximizing the coverage contribution of each sensor, followed by a consistency check for overlaps. If the overlap between two sensors exceeds a predefined threshold ϵ , the sensor with the smaller coverage contribution is reoriented toward its next-best candidate vertex. This reorientation process continues iteratively until the improvement in total network coverage between successive iterations falls below a specified tolerance level δ , ensuring computational convergence while maintaining high efficiency.

5.2. Case study: Voronoi-based coverage

To demonstrate the efficacy of the robustified orientation framework, we first analyze its performance under both nominal (best-case) and perturbed (worst-case) sensor placements. Figures 4a and 4b illustrate Voronoi diagrams corresponding to initial orientations and robustified orientations, respectively, for the best-case scenario in which all sensors are precisely located at their nominal positions. It is observed that the robustified orientation consistently directs sensors toward Voronoi vertices that enhance resilience against perturbations, thereby safeguarding coverage integrity. In contrast, initial orientations often lead to fragmented ground coverage, larger uncovered regions, and increased overlap among neighboring sensors, which collectively diminish the network's overall efficiency.

For theoretical deployments involving infinitely many sensors, the iterative process can be formally terminated once the incremental gain in total coverage between successive steps falls below a negligible threshold, effectively signifying convergence. In practical deployments, however, the number of available sensors m is finite and predetermined. In such cases, the optimization process naturally concludes once all sensors have either been oriented toward feasible vertices or placed into a non-active state. This ensures that the algorithm remains computationally efficient while adhering to realistic resource limitations.

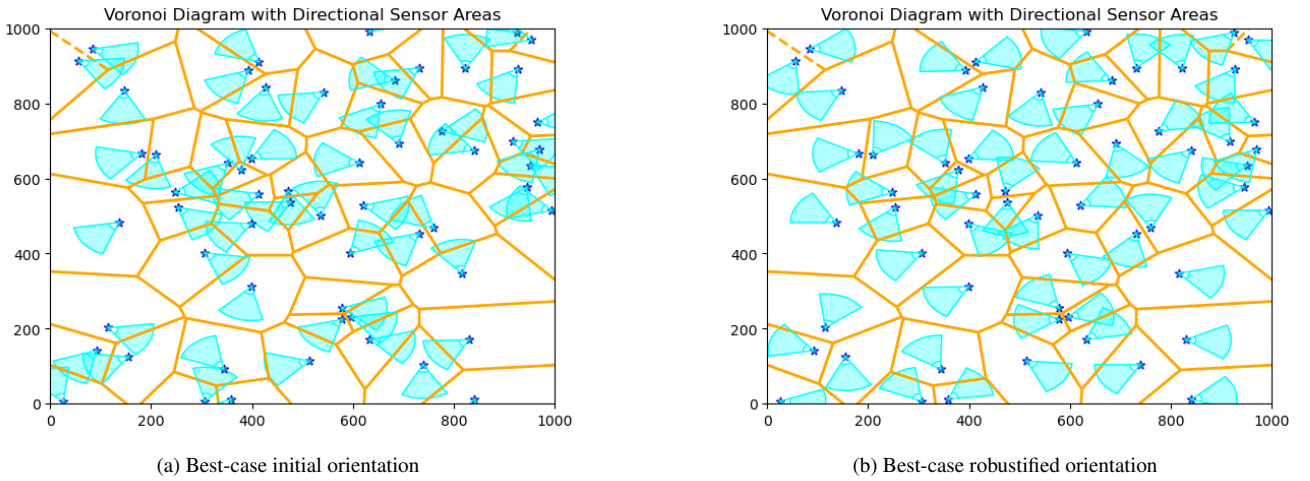


Figure 4: Voronoi diagrams showing coverage under best-case (nominal) sensor deployment.

To further assess performance under uncertainty, we consider the same nominal sensor positions but perturb their deployment locations to simulate worst-case conditions. Figures 5a and 5b present Voronoi diagrams under two contrasting cases: (i) coverage achieved through initial, unadjusted orientations and (ii) coverage obtained using robustified orientations. The robustified model demonstrates a consistent ability to preserve coverage even under significant perturbations, effectively reducing coverage fragmentation and overlap. In contrast, the random orientation strategy results in reduced uniformity and lower effective coverage across the monitored region. This disparity is particularly pronounced in the perturbed scenario, where the robustified orientation significantly

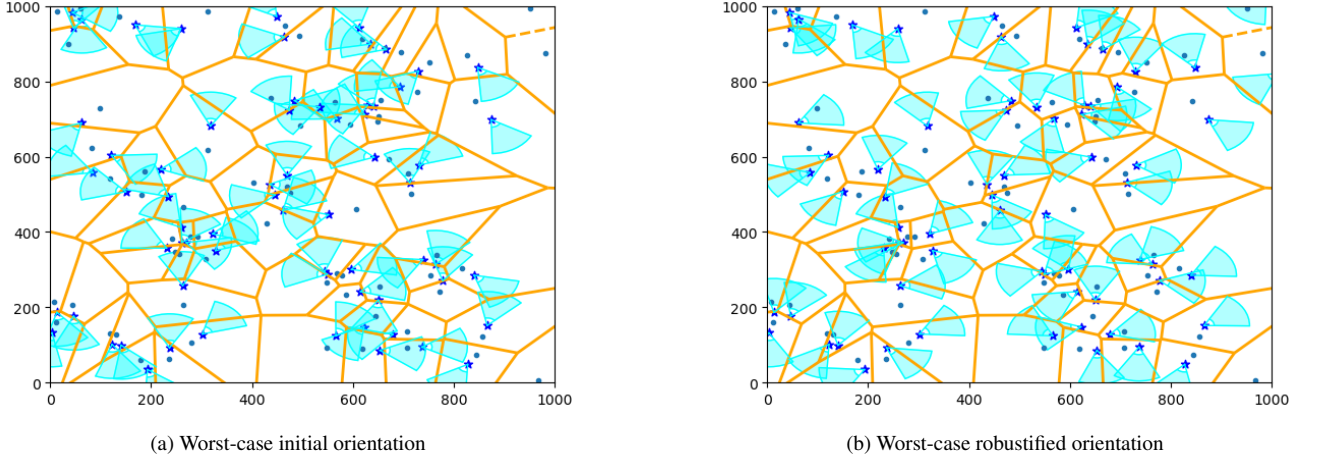


Figure 5: Voronoi diagrams showing coverage under worst-case (perturbed) sensor deployment.

outperforms the initial configuration. Repeated experiments over 1000 randomized sensor placements further confirm this trend: the average effective coverage under the initial orientation was only 31,584.37 square units, whereas the robustified orientation achieved a markedly higher average of 120,437.89 square units. These results compellingly demonstrate the robustness and scalability of the proposed framework in practical uncertain environments.

5.3. Comparative coverage analysis

We next present a comparative evaluation of the proposed robustified orientation strategy against two baseline methods: (i) random orientation, and (ii) IDS orientation, the latter being a deterministic vertex-based selection rule originally discussed in [7]. Figures 6a and 6b illustrate the corresponding coverage outcomes under both nominal (best-case) and perturbed (worst-case) deployment conditions. Under exact sensor locations, the results show that IDS and robustified orientations provide nearly identical coverage performance, with both significantly outperforming random orientation. The slight reduction in coverage observed for the robustified approach relative to IDS can be attributed to the conservative nature of solving the optimization model across the entire uncertainty set, rather than tailoring orientations solely to the nominal positions. This marginal trade-off represents the cost of achieving robustness, ensuring that sensor orientations remain resilient to deployment perturbations.

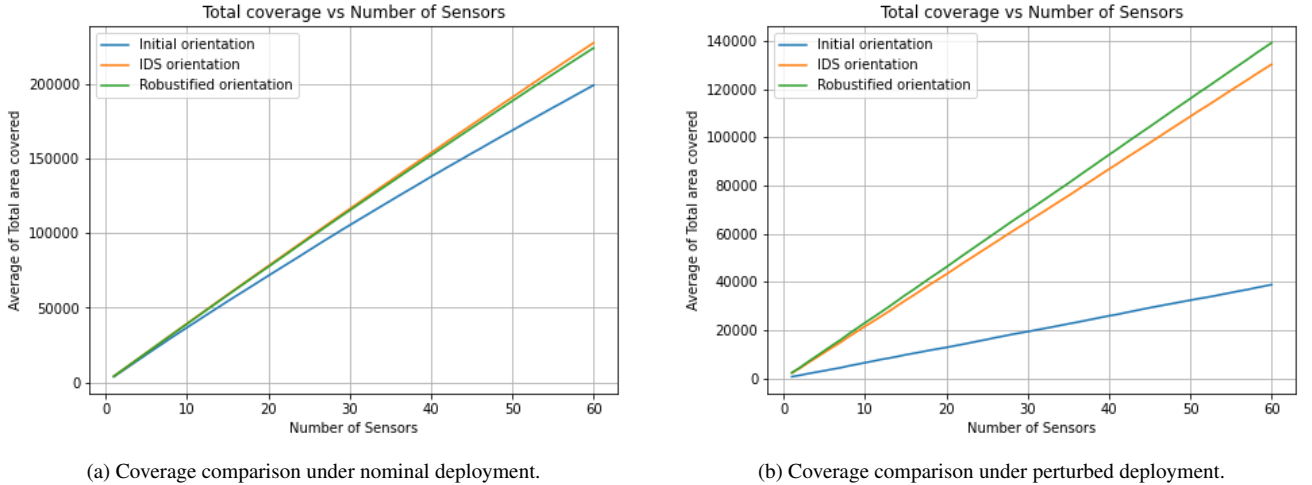


Figure 6: Coverage comparison (IDS, Random, and Robustified) for nominal (left) and perturbed (right) deployments.

When considering perturbed or worst-case sensor placements, the performance gap between IDS and the robustified orientation widens. As depicted in Figure 6b, IDS coverage deteriorates considerably when subjected to uncertainty, while the robustified approach consistently secures larger effective coverage areas. In sharp contrast,

random orientation yields highly irregular and sparse coverage patterns, performing so poorly that it becomes an unviable baseline for meaningful comparison. These findings highlight an important practical implication: in real-world scenarios where uncertainties in sensor placement are unavoidable, robustified orientation provides a reliable guarantee of satisfactory coverage, even if it entails a minor compromise in the best-case performance. From an operational standpoint, such guaranteed coverage is often more valuable than marginally higher nominal performance that fails to hold under perturbations, thereby underscoring the superiority of the robustified strategy for deployment in uncertain environments.

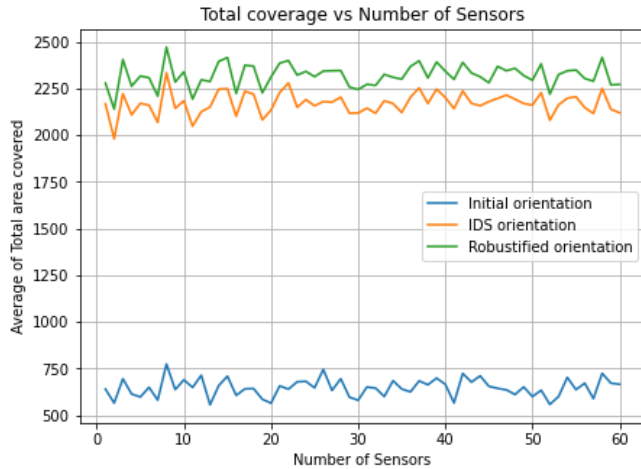


Figure 7: Voronoi-cell wise area distribution across sensors for different orientation strategies.

Figure 7 presents the Voronoi cell-wise area distribution across sensors under the three orientation strategies. The figure highlights a substantial disparity in the distribution of coverage: random orientation exhibits highly uneven allocation with several sensors covering negligible areas, while IDS demonstrates relatively better balance but still suffers degradation under perturbations. In contrast, the robustified approach produces consistently larger coverage across sensors, underscoring its effectiveness in safeguarding both individual sensor contributions and overall network resilience. The striking gap observed in Figure 7 reinforces that robustification not only enhances total coverage but also ensures equitable distribution, thereby establishing itself as the most reliable orientation strategy.

5.4. Parametric sensitivity analysis

We conclude our analysis by examining the robustness of the proposed framework under systematic variations of six key parameters, with one parameter perturbed at a time while the others are held fixed. The corresponding results are summarized in Table 1, which reports the total coverage achieved under robustified orientation for each parameter setting. This sensitivity study enables us to quantify how the network's performance responds to changes in deployment conditions and sensing characteristics, thereby providing deeper insights into the practical operating regime of the model. In essence, the analysis reports a similar comparison under different parameter configurations, confirming the consistency of the observed trend and highlighting the importance of carefully balancing sensing parameters in uncertain environments.

The most pronounced performance gain is observed when the horizontal sensing angle θ_H is widest, a result that is intuitively expected since larger angular views directly enlarge the sensing footprint. Nevertheless, practical deployments are often constrained by hardware cost and energy efficiency, necessitating a trade-off between maximizing coverage and minimizing resource expenditure. The impact of varying the number of sensors also reveals an interesting phenomenon: coverage initially increases as more sensors are deployed, but beyond a critical threshold, additional sensors contribute diminishing returns and in fact may lead to degradation due to excessive overlaps. This observation provides a valuable guideline for identifying an approximate upper bound on the number of sensors that should be deployed for cost-effective yet robust coverage.

We next investigate the effect of perturbation bounds, specifically the maximum and minimum values of ρ , which define the limits of the radius of robust feasibility. Varying the upper bound of perturbation does not

significantly alter the observed coverage, which suggests that in our experimental setting, the computed RRF was inherently smaller than the maximum perturbation considered. By contrast, increasing the lower bound of perturbation reduces the achievable coverage once a critical threshold is exceeded, reflecting the fact that stronger robustness requirements restrict feasible orientations. Finally, changes in the sensing range parameters exhibit the expected monotonic behavior: increasing the maximum sensing radius expands the area covered within each sensing cone, while enlarging the minimum radius shrinks the effective coverage. These findings are consistent across both nominal and perturbed deployments, as illustrated by comparative plots (Figure 7) that depict Voronoi cell-wise area distribution across sensors for different orientation strategies.

Table 1: Robustified total coverage under varying sensing parameters.

Parameter	Value Tested	Coverage	Parameter	Value Tested	Coverage
Number of sensors (m)	90	153224.8362	Minimum perturbation radius (ρ_{min})	10	165100.09529
	120	152302.18886		15	165100.09529
	150	155901.68308		20	165100.09529
	180	157546.81276		25	165100.09529
	360	157310.21007		30	164413.11907
Horizontal angle (θ_H)	30°	84770.68644		35	164515.22376
	60°	166058.19548		40	164422.47374
	90°	244356.8702	Maximum sensing range (R_s)	40	21939.11517
	120°	316347.876		50	50012.76467
	150°	379802.07159		60	84116.13499
	180°	432222.12524		70	123688.45844
	360°	614357.68854		80	165596.3334
Maximum perturbation radius (ρ_{max})	40	166761.81895		90	210448.34012
	50	166761.81895		120	338220.37022
	60	166761.81895	Minimum sensing range (r_s)	10	186612.39993
	70	166761.81895		15	182726.9938
	80	166761.81895		20	175882.99069
	90	166761.81895		25	166728.72809
	120	166761.81895		30	158362.75331
				35	147711.5152
				40	136367.46085

5.5. Key insights from experiments

The experimental analysis demonstrates that the RRF-based robustified orientation strategy consistently improves coverage over baseline methods, provides resilience under perturbations, and adapts effectively to variations in sensing parameters, thereby validating the practical utility of incorporating robustness constraints in aerial directional sensor networks. For nominal deployments, where sensors are placed at their exact intended locations, the coverage achieved by the initial orientation was 109,209.47 square units, while IDS orientation significantly improved performance to 206,829.61 square units; the robustified orientation achieved 201,815.78 square units, which is slightly lower than IDS but offers the critical advantage of robustness. In perturbed deployments representing worst-case sensor placements, the superiority of the robustified approach becomes more apparent: the coverage under initial orientation dropped drastically to 31,584.37 square units, IDS orientation improved performance to 111,505.36 square units, while the robustified orientation secured 120,437.90 square units, thereby outperforming both baselines. These results confirm that while IDS may marginally exceed robustified coverage under nominal conditions, the robustified framework guarantees consistently higher and more reliable coverage in uncertain scenarios, highlighting its effectiveness as a resilient orientation strategy for aerial directional sensor networks.

6. Conclusion and future work

This paper introduces a unified framework combining location uncertainty, robustness, the radius of robust feasibility and 3D directional sensing for aerial sensor networks. By embedding RRF into the coverage model, we develop both robust and RRF-constrained formulations, enabling orientations resilient to worst-case displacements. The iterative procedure: optimizing, computing RRF, and re-optimizing if necessary, proves resource efficiency and improves coverage while controlling overlaps. Simulations show RRF-based orientations outperform in robustness and coverage retention without probabilistic assumptions. Future work includes real-time distributed implementations, integration with mobile sensing and handling compound uncertainties. Extending the framework to multi-objective settings (coverage, energy, latency) further enhances its applicability to broader uncertainty-aware sensing problems.

References

- [1] Li, W., Wang, X., Han, S.: Coverage enhance in boundary deployed camera sensor networks for airport surface surveillance. *IEEE Access*. **9**, 145728-145738 (2021)
- [2] Liang, J. M., Mishra, S., Lin, C. H.: Enhanced PTZ Camera Dispatch Scheme for 3D Environments Based on Deep Reinforcement Learning. *IEEE Transactions on Instrumentation and Measurement*, IEEE. (2025)
- [3] Ye, W., Ordonez, F.: Robust optimization models for energy-limited wireless sensor networks under distance uncertainty. *IEEE transactions on wireless communications*, IEEE. **7**(6), 2161-2169 (2008)
- [4] Sangwan, A., Singh, R. P.: Survey on coverage problems in wireless sensor networks. *Wireless Personal Communications*, Springer. **80**, 1475-1500 (2015)
- [5] Adachi, T., Hayashi, N. Takai, S.: Cooperative target tracking by multiagent camera sensor networks via Gaussian process. *IEEE Access*, IEEE. **10**, 71717-71727 (2022)
- [6] Li, Chen, H.: UAV enhanced target-barrier coverage algorithm for wireless sensor networks based on reinforcement learning. *Sensors*, MDPI. **22**(17), 6381 (2022)
- [7] Sung, T. W., Yang, C. S.: Voronoi-based coverage improvement approach for wireless directional sensor networks. *J. Netw. Comput. Appl.* **39**, 202-213 (2014)
- [8] Wang, Y., Wu, S., Chen, Z., Gao, X., Chen, G.: Coverage problem with uncertain properties in wireless sensor networks: A survey. *Computer Networks*, Elsevier **123**, 200–232 (2017)
- [9] Erişkin, L.: Point coverage with heterogeneous sensor networks: A robust optimization approach under target location uncertainty. *Computer Networks*, Elsevier. **198** (108416), (2021)
- [10] Thomas, D., Shankaran, R.,: A secure barrier coverage scheduling framework for WSN-based IoT applications. *Proceedings of the 23rd International ACM Conference on Modeling, Analysis and Simulation of Wireless and Mobile Systems*. 215-224 (2020)
- [11] Mahfouz, A. M., Ismail, A. S., El Sobky, W. I., Nasry, H.: A novel model for representing a plane target and finding the worst-case coverage in wireless sensor network based on Clifford algebra. *EURASIP Journal on Wireless Communications and Networking*, Springer. **2023** (1), 95 (2023)
- [12] Luo, C., Hong, Y., Li, D., Wang, Y., Chen, W., Hu, Q.: Maximizing network lifetime using coverage sets scheduling in wireless sensor networks. *Ad Hoc Networks*, Elsevier. **98**, 102037 (2020)
- [13] Thammawichai, M., Luangwilai, T.: An energy-optimization topology control for three-dimensional wireless sensor networks. *Journal of Communications and Networks*, KICS. **25**(6), 778-788 (2023)

- [14] Ben-Tal, A., El Ghaoui, L., Nemirovski, A.: Robust Optimization. Princeton University Press, Princeton (2009)
- [15] Kouvelis, P., Yu, G.: Robust Discrete Optimization and Its Applications. Springer, Berlin (2013)
- [16] Soyster, A.L.: Convex programming with set-inclusive constraints and applications to inexact linear programming. *Oper. Res.* **21**(5), 1154-1157 (1973)
- [17] Ben-Tal, A., Nemirovski, A.: Robust solutions of linear programming problems contaminated with uncertain data. *Math. Program.* **88**, 411-424 (2000)
- [18] Bertsimas, D., Sim, M.: The price of robustness. *Operations research, Informs.* **52**(1), 35-53 (2004)
- [19] Ben-Tal, A., den Hertog, D., Vial, J.-P.: Deriving robust counterparts of nonlinear uncertain inequalities. *Math. Program. Ser. A* **149**(1-2), 265-299 (2015)
- [20] Ben-Tal, A., Nemirovski, A., Roos, C.: Robust solutions of uncertain quadratic and conic-quadratic problems. *SIAM J. Optim.* **13**(2), 535-560 (2002)
- [21] Leyffer, S., Menickelly, M., Munson, T., Vanaret, C., Wild, S.M.: A survey of nonlinear robust optimization. *INFOR Inf. Syst. Oper. Res.* **58**(2), 342-373 (2020)
- [22] Boyd, S., Vandenberghe, L.: Convex Optimization. Cambridge University Press, Cambridge (2004)
- [23] Gabrel, V., Murat, C., Thiele, A.: Recent advances in robust optimization: An overview. *European J. Oper. Res.* **235**(3), 471-483 (2014)
- [24] Goberna, M.A., Jeyakumar, V., Li, G., Vicente-Pérez, J.: Robust solutions of multiobjective linear semi-infinite programs under constraint data uncertainty. *SIAM J. Optim.* **24**(3), 1402-1419 (2014)
- [25] Dinh, N., Goberna, M. A., López C. M. A.: From linear to convex systems: Consistency, Farkas' lemma and applications. *Journal of Convex Analysis*, Heldermann Verlag. **13**(1), (2006)
- [26] Goberna, M.A., Jeyakumar, V., Li, G., Vicente-Pérez, J.: The radius of robust feasibility of uncertain mathematical programs: A Survey and Recent Developments. *European J. Oper. Res.* **296**(3), 749-763 (2022)
- [27] Eren, O., Altin K.A.: A simulation-informed robust optimization framework for the design of energy efficient underwater sensor networks. *Ad Hoc Networks*, Elsevier. 103933 (2025)
- [28] Ridolfi, A.B., Vera de Serio, V.N.: A Radius of Robust Feasibility for Uncertain Farthest Voronoi Cells. *Set-Valued Var. Anal.* **31**(1) (2023)
- [29] Datta, V., Nahak, C.: A Radius of Robust Feasibility Approach to Directional Sensors in Uncertain Terrain. *arXiv preprint arXiv:2510.19407*, 2025.
- [30] Goberna, M.A., Jeyakumar, V., Li, G., Vicente-Pérez, J.: Robust solutions to multi-objective linear programs with uncertain data. *European J. Oper. Res.* **242**(3), 730-743 (2015)
- [31] Goberna, M.A., Jeyakumar, V., Li, G., Linh, N.: Radius of robust feasibility formulas for classes of convex programs with uncertain polynomial constraints. *Oper. Res. Lett.* **44**(1), 67-73 (2016)
- [32] Chuong, T., Jeyakumar, V.: Robust global error bounds for uncertain linear inequality systems with applications. *Linear Algebra and its Applications*, Elsevier. **493**, 183-205 (2016)
- [33] Chen, J., Li, J., Li, X., Lv, Y., Yao, J.C.: Radius of robust feasibility of system of convex inequalities with uncertain data. *J. Optim. Theory Appl.* **184**(2), 384-399 (2020)

[34] Li, X.B., Wang, Q.L.: A note on the radius of robust feasibility for uncertain convex programs. *Filomat* **32**(19), 6809-6818 (2018)

[35] Wang, M., Li, X. B., Chen, J., Al-Homidan, S.: On radius of robust feasibility for convex conic programs with data uncertainty. *Numerical Functional Analysis and Optimization*, Taylor & Francis. **42**(16), 1896-1924 (2022)

[36] Goberna, M. A., Jeyakumar, V., Li, G.: Calculating radius of robust feasibility of uncertain linear conic programs via semi-definite programs. *Journal of Optimization Theory and Applications*, Springer. **189**(2), 597-622 (2021)

[37] Chuong, T.D., Jeyakumar, V.: An exact formula for radius of robust feasibility of uncertain linear programs. *J. Optim. Theory Appl.* **173**(1), 203-226 (2017)

[38] Chuong, T. D.: Radius of robust global error bound for piecewise linear inequality systems. *Journal of Optimization Theory and Applications*, Springer. **191**(1), 68-82 (2021)

[39] Sun, X., Xiao, C., Guo, X.: Radius of Robust Feasibility for Adjustable Robust Linear Inequality Systems with Affine Decision Rules. *Bulletin of the Malaysian Mathematical Sciences Society*, Springer. **48**(4), 92 (2025)

[40] Tan, W., Guo, X., Sun, X.: On Robust Global Error Bounds for a Class of Uncertain Piecewise Linear Inequality Systems. *Axioms*, MDPI. **11**(10), 497 (2022)

[41] Liers, F., Schewe, L., Thürauf, J.: Radius of robust feasibility for mixed-integer problems. *INFORMS Journal on Computing*, INFORMS. **34**(1), 243-261 (2022)

[42] Goberna, M. A., Jeyakumar, V., Li, G., Pérez, J. V.: Guaranteeing highly robust weakly efficient solutions for uncertain multi-objective convex programs. *European Journal of Operational Research*, Elsevier. **270**(1), 40-50 (2018)

[43] Goberna, M.A., López-Cerdá, M.A.: *Linear Semi-Infinite Optimization*. Wiley, Chichester (1998)